Cu-modified Ni foams as three-dimensional outer anodes for high-performance hybrid direct coal fuel cells

Heping Xie[1, 2, *], Shuo Zhai[1, 2], Tao Liu[1], Hailong Liao[1], Yuan Zhang[3], Wei Zhou[3], Zongping Shao[3], Meng Ni[4], Bin Chen[2]

[1]Institute of New Energy and Low-Carbon Technology, Sichuan University, Chengdu 610065, China.

[2]Guangdong Provincial Key Laboratory of Deep Earth Sciences and Geothermal Energy Exploitation and Utilization, Institute of Deep Earth Sciences and Green Energy, Shenzhen University, Shenzhen 518060, China.

[3]State Key Laboratory of Materials-Oriented Chemical Engineering, College of Chemical Engineering, Nanjing Tech University, Nanjing 210009, China.

[4]Building Energy Research Group, Department of Building and Real Estate, The Hong Kong Polytechnic University, Hung Hom, Kowloon, Hong Kong, China.

[*]**Corresponding author**

Email address: xiehp@scu.edu.cn

Abstract

The hybrid direct coal fuel cell is a promising technology for the generation of power using coal, which is abundant and cheap. However, restricted contact between the solid carbon in the coal and the anode of the cell not only limits the electrochemical oxidation sites, but also adversely affects the transport of electrons and ions. Herein, we demonstrate a new strategy of using Cu-modified Ni foams as the three-dimensional outer anode for a high-performance hybrid direct coal fuel cell with 3D structure, that is rich in electrochemical reaction sites and beneficial for electron and ion transport when filled with molten carbonates and anthracite coal. Moreover, the CuNi alloy layer formed on the surface of Ni foam is of excellent coking-resistance and capable of preventing ash-clogging, therefore effectively promoting the durability of an electrolyte-supported HDCFC. An excellent maximum power density of 378 mW cm^{-2} at 750 °C is achieved using the prepared 3D anode and anthracite coal as fuel. Besides, the cell exhibited stable operation for more than 13 h at 100 mA cm^{-2}, promising a new electrode design strategy for developing high-performance HDCFC anodes.

Keywords:

1. Introduction

Coal, an abundant and competitive fuel, is expected to maintain dominance in the power generation industries of developing countries due to its superior high energy density and friendliness for storage and transportation [1-3]. However, developing highly efficient and environmentally-benign coal utilization technology remains a challenge [4-6]. Direct carbon fuel cells (DCFCs) have attracted considerable attention as a promising option that directly converts the chemical energy of carbon into electricity without the Carnot cycle. Thus, DCFCs have high energy efficiency, close to 100% in theory [7-10]. Up to now, DCFCs can be divided into four general types, according to the type of electrolyte: molten carbonate fuel cells (MCFCs), molten hydroxide fuel cells (MHFCs), solid oxide electrolyte fuel cells (SOFCs), and the newly-developed hybrid direct carbon fuel cells (HDCFCs), which add molten carbonates to the solid carbon to form the hybrid electrolyte in together with the solid electolyte (e.g. stablized Yitrium oxides, doped cerium oxides) within the traditional SOFC configuration [11-12]. Therefore, for HDCFCs, ion transportation is enhanced by the molten ion-conducting carbonates. In addition, gasification of the carbon can be faciliated in molten carbonates and the electrochemical oxidation sites can also be expanded from the solid carbon/anode interface to the molten carbonate/carbon interface due to the increased contact [13-14]. Recently, numerous efforts have been focus on designing characteristic anode structure or morphology which is considered as an effective way to regulate the electrochemical oxidation sites of carbon [15]. Liu and co-workers demonstrated a $Ce_{0.6}Mn_{0.3}Fe_{0.1}O_2$ hierarchically structured porous hollow nanofibers which can be customized as efficient anodes for HDCFCs [16]. Wu and co-workers proposed a highly efficient, 3D solid-state architected Ni-GDC anode using textile as framework [17]. Ma and co-workers developed a honeycombed and size-matching $(PrBa)_{0.95}Fe_{1.4}Cu_{0.4}Nb_{0.2}O_{5+d}$ anode anode architecture by using water droplet templating method for high performance hybrid direct carbon fuel cells [18]. However, due to the poor electron conductivity of molten carbonate, efficient direct electrochemical oxidation of carbon in HDCFCs is still a challenge.

One solution to this electron transport issue is to build a three-dimensional (3D) electron-conductive anode with rich contacts with the fuel-carbonate mixture, which allows for

rapid electron transfer. Metal foam is a very attractive material due to its excellent electrical conductivity, high mechanical strength, and large specific surface area [19]. Therefore, it is widely used in the field of electrochemistry, for example in gas-fueled SOFCs [20], zinc-air batteries [21], and lithium ion batteries [22]. Nickel foam in particular has been used commercially as an electrode substrate and current collector for nickel-based alkaline batteries for more than 20 years [23]. Other benefits of nickel foam, such as its good electrochemical catalytic carbon oxidation activity and stability in a reducing gas atmosphere, also make it attractive as a current collector in SOFCs. Unfortunately, ni easily suffers from coking in the absence of decoking agents (e.g., H_2O, CO_2, catalysts) at HDCFC operating temperatures, increasing the ohmic impedance and decreasing the catalytic activity of nickel [24]. Therefore, nickel foam should be modified to achieve an excellent tolerance to carbon deposition in HDCFCs.

Herein, the strategy of using metal foam as the 3D outer anode for HDCFCs is developed for the first time. The electrochemical properties of anthracite-fueled HDCFCs using Ni foam with different porosities were investigated. finding the foam with a mesh density of 90 PPI showed the best performance in the fuel cell, as an successful demonstration of the extended reaction sites, enhanced electron conducting, synergetically. Furthermore, the formation of a CuNi alloy layer on the surface of Ni foam via electrodeposition and reduction endows the cell excellent coke-resistance, which ahcieved a maximum power density of 378 mW cm^{-2} at 750 °C and stable discharge for more than 13 h with 0.6 g coal-carbonate mixture as the fuel.

2. Experimental

2.1. Material preparation and characterization

All commercial reagents were analytical grade and purchased from Aladdin Reagents. Both the $SrSc_{0.175}Nb_{0.025}Co_{0.8}O_{3-d}$ (SSNC) and $Sm_{0.2}Ce_{0.8}O_{1.9}$ (SDC) composite oxide powders used in this work were prepared via an EDTA-citrate method; the detailed synthesis process is described elsewhere [25]. Phase-pure powders were obtained by calcination of SSNC and SDC precursors at 900 °C and 700 °C, respectively, in air for 5 h.

The Ni foams were commercial products from Yinghuixiong Electronic Materials Co., Ltd., with a pore per linear inch (PPI) value of 30 and 90. Before use, the nickel foam was cut into cylinders

with diameters of 9 mm and heights of 3 mm, then rinsed with acetone and alcohol and dried in air at 80 °C for 1 h. The Cu-modified Ni foam was obtained via typical electrodeposition. A three-electrode system was used with the Ni foam, a copper sheet and SCE (saturated calomel electrode) served as a work electrode (WE), counter electrode (CE), and reference electrode (RE), respectively. The electrodeposition solution contained 1M $CuSO_4$ and 0.001M polyvinylpyrrolidone (PVP). The deposition current density was held constant at -1 A cm^{-2}, and the deposition area was 1.3 cm^2. After 10 min, the mass loading reached 200 mg cm^{-2}. Finally, the bare Ni foams and Cu-modified Ni foams were heated at 800 °C for 5 h in 10% H_2 (balanced with Ar) before the electrochemical performance and stability tests.

Analysis using a scanning electron microscope (SEM, FEI Inspect F50, USA) equipped with an energy dispersive spectrometer (EDS) was performed to characterized the morphologies of the metal foams. X-ray diffraction (XRD, Bruker AXS D8 Advance A25X) analysis was used to examine the crystal structure of the metal foams.

After reduction, the Ni foam and Cu-modified Ni foam were immersed in a mixture of anthracite and carbonate at 750 °C for 20 h in N_2 to compare their coke resistance. Before testing, the metal foams were rinsed with acetone and alcohol throughly, then dried at 80 °C in air for 1 h. Then Raman experiments were conducted with a Renishaw inVia Reflex, using an excitation wavelength of 532 nm. O_2 temperature-programmed oxidation (O_2-TPO) was conducted in an AutoChem1 II 2920. Prior to testing, the metal foams were crumbled to powder, which was put into a U-type quartz reactor where pure O_2 was purged at a flow rate of 20 mL min^{-1}. For each test, the sample was heated from 50 °C to 900 °C at a heating rate of 10 °C/min, and the CO_2 produced by the oxidation of the coke was detected as TCD signals by chemisorption. After immersion in the mixture of anthracite and carbonate, the morphologies of the metal foams were examined by SEM.

2.2. Cell fabrication

The single fuel cell consists of a Foam|NiO-SDC|YSZ|SDC|SSNC five-layer structure. A yttria-stabilized zirconia (YSZ) electrolyte support with a mass of 0.2 g was prepared by dry-pressing uniaxially at 100 MPa, followed by sintering at 1450 °C for 5 h to be 200 μm in thickness. A thin-film SDC interlayer (~4 μm) was deposited onto one side of the YSZ electrolyte and then sintered at 1250 °C for 5 h. Mixtures of NiO and SDC powder (weight ratio of 6:4) were

dispersed in isopropyl alcohol to form a suspension which was sprayed onto the other side of the YSZ electrolyte. Then, SSNC cathode ink was sprayed onto the SDC interlayer, with an effective surface area of 0.45 cm^{-2}, and calcined at 1100 °C for 2 h. Finally, the metal foam was attached to the Ni/SDC anode by silver paste (DAD-87, Shanghai) to form five-layer structure. It's worth noting that silver pasta was painted in a net shape on the surface of Ni/SDC anode as a current collector and binding the metal foam to the Ni/SDC anode. The fabrication process of the button cell is summarized in Fig. 1a.
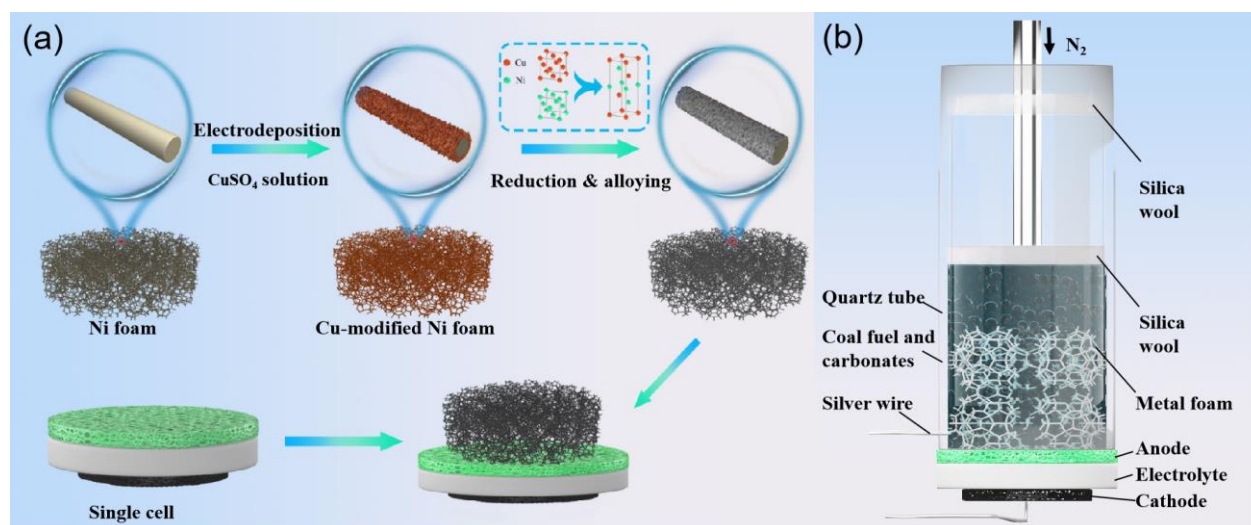

Fig. 1. (a) Fabrication process for Cu-modified Ni foam as a 3D anode, and (b) schematic diagram of the coal-fueled single HDCFC.

2.3 Fuel preparation and characterization

Anthracite (Yangquan Coal Industry Co. Ltd, China) passed through a 250-mesh sieve was used as fuel for the HDCFC in this work. The composition of the anthracite was determined by proximate analysis (wt% of moisture, ash, volatiles, and fixed carbon) and ultimate analysis (wt% of C, H, O, N, and S) and is shown in Table 1. The proximate analysis was performed according to the Standard GB/T212 of China. The ultimate analysis of the organic elements was carried out using a Vario EL cube. The result shows that the content of fixed carbon and ash were 81.91% and 11.03%, respectively. The composition of the ash, which was examined via X-ray fluorescence (XRF, Axios max), is listed in Table 2.

Table 1

Proximate and ultimate analyses of anthracite.

	Proximate analysis (wt.%, air dry basis)				Ultimate analysis (wt.%, air dry basis)				
	Moisture	Ash	Volatiles	Fixed carbon	C	H	O	N	S
anthracite	0.63	11.03	6.43	81.91	82.32	2.81	4.59	1.15	0.13

Table 2

Ash composition of the anthracite (wt.%).

SiO_2	Al_2O_3	Fe_2O_3	SO_3	CaO	TiO_2	P_2O_5	SrO	Na_2O	MgO	V_2O_5	Cl	K_2O
29.41	27.66	13.62	10.17	5.10	4.24	3.87	2.56	1.08	0.69	0.66	0.63	0.33

A mixture of coal and carbonate (containing 62 mol% lithium carbonate and 38 mol% potassium carbonate) with a weight ratio of 7:3 was prepared by the ball milling method. The mixture was dried at 80 °C and sieved with a 250-mesh steel sieve before it was added to the cell.

2.4 HDCFC assembly and testing

Silver wires were attached to the metal foam and to the cathode after painting the cathode with silver paste to collect electrons. The button cell was sealed to a quartz tube with silver paste, as shown in Fig. 1b. Then, 0.6 g of the coal-carbonate mixture was added to the anode chamber without any carrier gas; ambient air was used in the cathode side. A Solartron 1287 Electrochemical Workstation was used to test the electrochemical performance of the HDCFC. In the electrochemical impedance spectra test, the voltage amplitude was 30 mV in the frequency range from 0.1 Hz to 100 kHz.

3. Results and discussions

3.1 Reaction characteristics of Ni foam as the three-dimensional outer anode

As shown in Fig. 2, restricted contact between carbon and the two-dimensional (2D) Ni/SDC

inner anode not only restricts electrochemical oxidation sites to the two-dimensional surface, but also adversely affects electron transport in electrochemical reactions [26]. With the addition of metal foam, the sifted molten carbonate and carbon can easily pass through the large pores of the metal foam to form a 3D metal/carbonate outer anode. This design expands the sites of direct electrochemical oxidation of carbon from the 2D interface of the carbon/anode to the entire 3D space where the foam metal is located; this promotes the direct electrochemical oxidation of carbon, thus improving the electrochemical performance of HDCFCs.
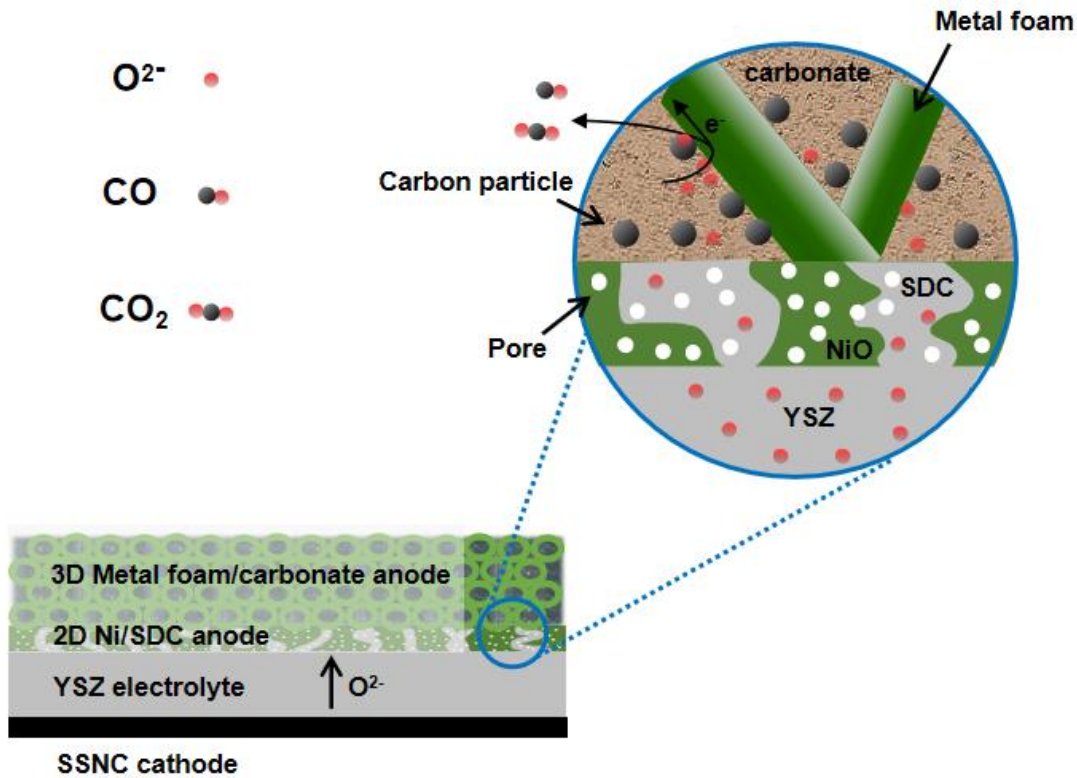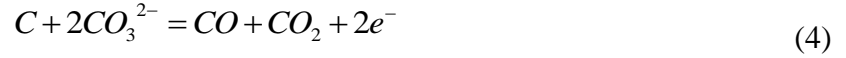

Fig. 2. Electrochemical processes at the electrolyte/electrode interface.

As shown in Fig. 1b. Under the press of the intake quartz pipe and gravity, the fuel can maintain a stable contact with the anode, which is vital for the outer anode. In this cell configuration, the anodic reaction can be expressed as follows: (i) electrochemical oxidation of carbon by O^{2-} ions (Eq. (1) and Eq. (2)); (ii) electrochemical oxidation of carbon by CO_3^{2-} via Eq. (3) and Eq. (4); (**iii**) the electrochemical oxidation of CO via Eq. (5) and Eq.(6), mainly driven by the reversed Boudouard reaction (Eq. (7) [27-29].

$$C + 2O^{2-} = CO_2 + 4e^-$$ (1)

$$C + O^{2-} = CO + 2e^-$$ (2)

$$C + 2CO_3^{2-} = 3CO_2 + 4e^-$$ (3)

$$C + 2CO_3^{2-} = CO + CO_2 + 2e^-$$ (4)

$$C + CO_2 = 2CO$$ (5)

$$CO + O^{2-} = CO_2 + 2e^-$$ (6)

$$CO + CO_3^{2-} = 2CO_2 + 2e^-$$ (7)

For HDCFCs, the most commonly used fuels are activated carbon [30] and carbon black [31], which are of smaller density than that of carbonate, thus may float to the top of molten carbonate during operation; this limits the contact of carbon fuel and ion-conducting phase [32]. In this work, anthracite, a real raw coal of a larger density due to its high graphitization and metallic impurities, was used to aviod this issue [33].

To determine the influence of the metal foam on the cells, two different sizes of Ni foam (30 PPI and 90 PPI) were used. Fig. 3 shows the surface morphology, characterized by SEM, of the Ni foams after reduction at 800 °C in H_2 atmosphere. The low-resolution scanning electron microscope images shows that the pore diameters of the 30 PPI Ni foam (Fig. 3a) and 90PPI Ni foam (Figs. 3b) were approximately 1 mm and 0.3 mm, respectively; this was much higher than the particle size of the sieved coal (250 mesh, 0.065 mm), which ensured that the anthracite particles could migrate through the Ni foams continuously during fuel consumption, maintaining good contact between the Ni/SDC layer and the fuel. After reduction at high temperature, Ni foams all retained their original shape, exhibiting good mechanical strength when subject to chemical and thermal stress.
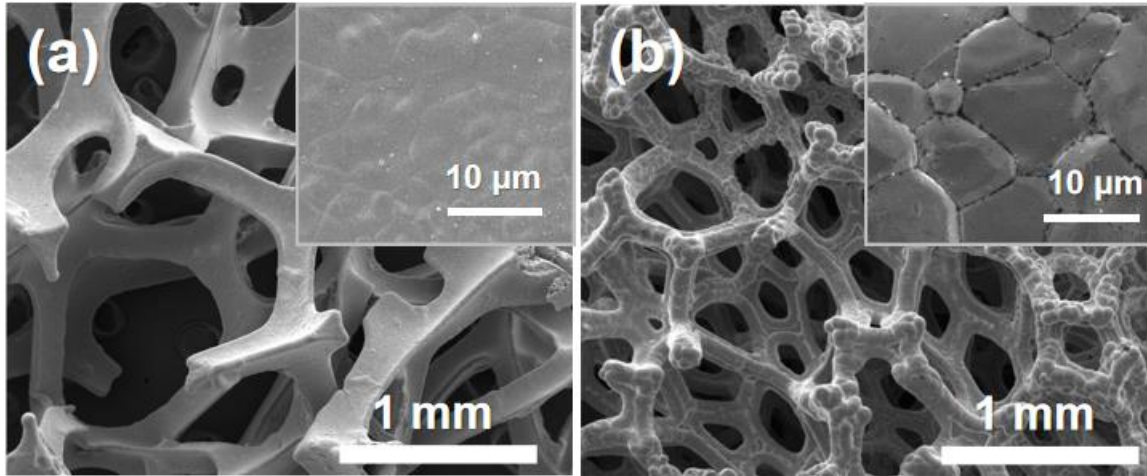
Fig. 3. SEM images of (a) 30 PPI Ni foam, (b) 90 PPI Ni foam after H_2 reduction.

Fig. 4 compares the electrochemical performances of HDCFCs without and with Ni foams. Fig. 4a shows the current density–voltage (I–V) curves and current density–power density (I–P) curves of the HDCFCs. The open circuit voltages are all close to the theoretical value of 1.03 V, indicating high electrolyte density and good tightness of the cells [34]. The maximum power density of the cell with 90 PPI Ni foam was 389 mW cm^{-2}, higher than the cells with 30 PPI Ni foam (349 mW cm^{-2}) and without Ni foam (306 mW cm^{-2}). Fig. 4b shows the impedance spectra (EIS) of the HDCFCs; the values of ohmic resistance (R_o) and polarization resistance (R_P) are shown in the inset histogram. The R_o values are almost identical, indicating the same electrolyte thickness in different cells. Considering that the configuration of the cells was the same except for the metal foam, the difference in R_P was mainly caused by the change of anodic polarization with (out) metal foam. In an increasing order, the R_P values were 0.34 Ω cm^2 (90 PPI Ni foam), 0.42 Ω cm^2 (30 PPI Ni foam), and 0.60 Ω cm^2 (without Ni foam); this is consistent with the maximum power density results. In addition, the low frequency arc of the EIS tended to be suppressed in the cells with the Ni foam. Since the the low frequency arc is related to mass transport, the 3D metal/carbonate contact can be deemed to reduce the carbon travel distance by extending the reaction sites to the whole foam layer, as well as the enlarged electrochemical sites for carbon.
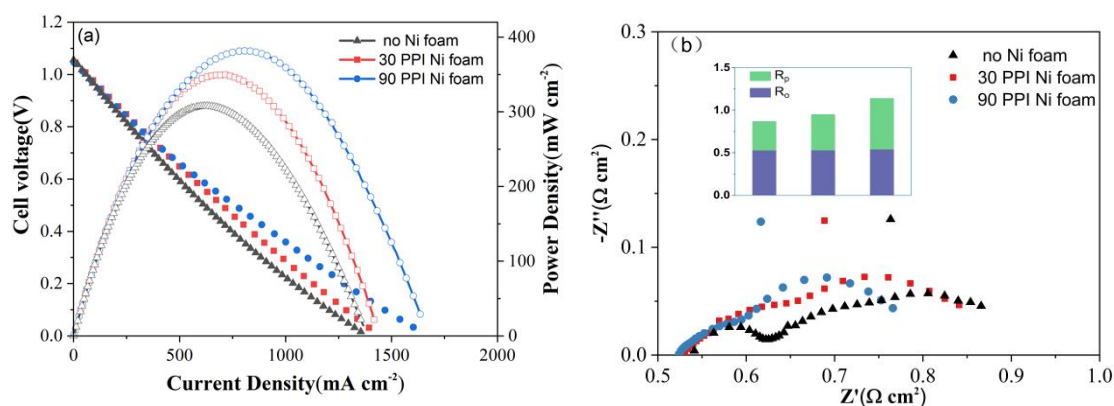
Fig. 4. Performance of HDCFCs without Ni foam, with 30 PPI Ni foam, and with 90 PPI Ni foam at 750 °C. (a) I–V and I–P curves, (b) EIS under OCV with the corresponding ohmic resistance (R_o) and polarization resistance (R_P) (inset).

3.2 Electrochemical performances of the Cu-Modified Ni Foams as Three-Dimensional Outer Anodes

As known, Ni is prone to be carbon-deposited at high temperature in environment of hydrocarbon fuels, particularly coal; carbon deposition not only impedes electron transport but also blocks catalytic sites on the surface [35]. In order to improve the durability of the Ni foam as well as the whole cell, we modified its surface with copper, a highly conductive and carbon-resistant metal by a facile electrodeposition method [36]. Fig. 5 shows SEM images and XRD analysis results of the reduced Cu-modified Ni foam. As shown in Fig. 5a, after electrodeposition, the Ni foam was evenly coated by Cu without dendrites observed. In Fig. 5b, the reduced Cu-modified Ni foam shows a smooth surface morphology and clear grain boundaries due to the recrystallization processes. Fig. 5c shows elemental maps from an area in the reduced Cu-modified Ni foam, displaying a highly uniform distribution of both Ni and Cu. In addition, the corresponding EDS spectra in Fig. 5d indicate that the content of Cu of the surface coverage was more than 20%, although the concentration of Cu decreases with the depth into the Ni [37]. Fig. 5e shows the XRD patterns, used to examine the phase of Ni and Cu of the metal foams. The Ni foam displayed a single metallic Ni phase (PDF # 01-088-2326), while the Cu-modified Ni foam showed an additional peaks of copper (PDF #01-089-2838) after Cu deposition. After reducing in H_2 atmosphere at 800 °C, intermetallic CuNi and a small amount of Ni were observed in the reduced Cu-modified Ni foam according to emerged peak of CuNi located between the Ni and

Cu .It can be explained by the diffusion of deposited Cu atoms into the Ni substrate and the subsquent alloying,which is well verified in literature [38]. All of them showed three characteristic reflections at $2\theta = 44.15-45.50°$, $2\theta = 51.36-52.84°$ and $2\theta = 74.80-77.22°$, which were ascribed to (111), (200) and (220) crystal planes of face-centred cubic (fcc) structure [39].
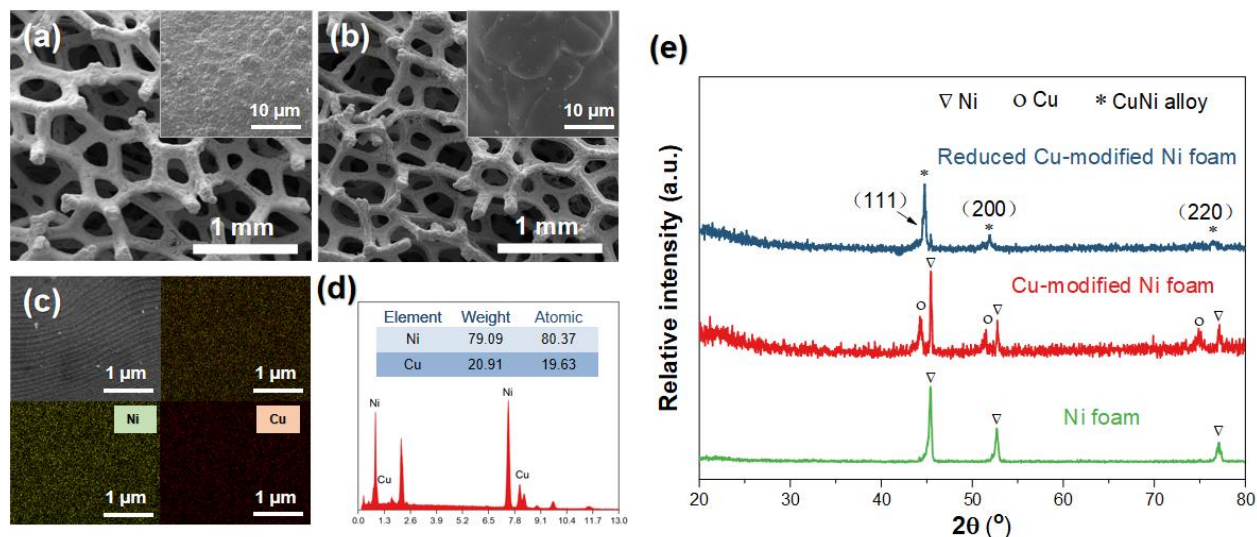

Fig. 5. SEM images of (a) Cu-modified Ni foam and (b) reduced Cu-modified Ni foam. (c) Elemental maps of reduced Cu-modified Ni foam. (d) The corresponding EDS spectra. (e) XRD patterns of Ni foam (green), Cu-modified Ni foam (red), and reduced Cu-modified Ni foam (gray).

To compare the coking resistance of the Ni foam and the Cu-modified Ni foam, Raman spectroscopy, O_2-TPO experiments and SEM imaging were performed for foams after immersing the samples in the anthracite-carbonate mixture at 750 °C for 20 h. As shown from the Raman shift results in Fig. 6a, two distinct bands representing coke (C-C), at 1350 cm^{-1} (the D-band) and 1580 cm^{-1} (the G-band) respectively, were observed for the Ni foam; in contrast, only weak peaks were observed for the Cu-modified Ni foam, which clearly indicate the improved coke-resistance after Cu modification [40]. From the O_2-TPO profiles, shown in Fig. 6b, the intensity of CO_2 peaks for the Ni foam and Cu-modified Ni foam, again, reveals that more amount of carbon deposited on the Ni foam. This result is consistent with the conclusions of previous experiments which demonstrate that the introduction of Cu improves coking resistance [41].

The morphologies of the Ni foam and Cu-modified Ni foam after the tests are shown in Fig. 6c and Fig. 6d, respectively. It can be seen a large amount of carbon was deposited on the nickel

foam skeleton, and its surface was corroded with pores by the coal attack. In contrast, only a small amount of coke could be seen on the skeleton of the Cu-modified Ni foam, and there was no sign of corrosion on its surface. In this regard, modifying the surface of the Ni foam significantly prevents the corrosion and carbon deposition in the HDCFCs, thus being a very facile and effective method to improve the cell durability.
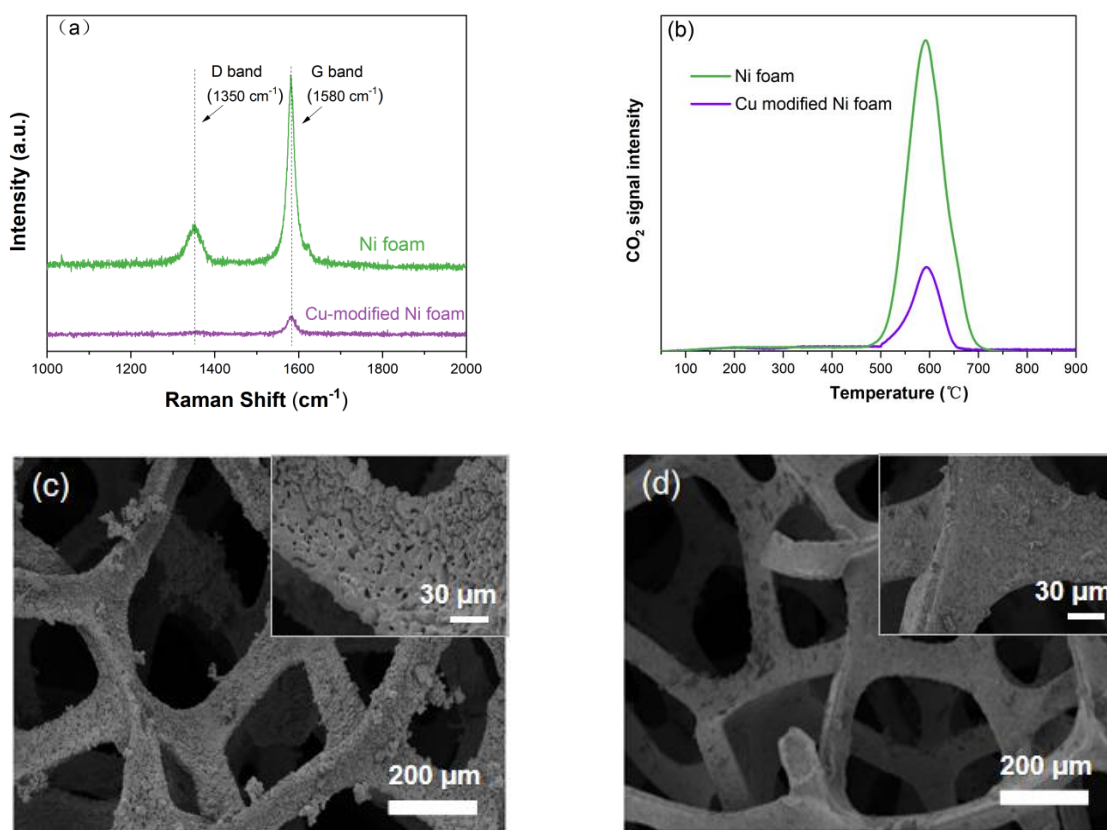

Fig. 6. (a) Raman spectra and (b) O_2-TPO curves. (c and d) SEM images of Ni foam and Cu-modified Ni foam after immersion in the anthracite-carbonate mixture at 750 °C for 20 h.

Fig. 7a shows the electrochemical performances of the HDCFC using Cu-modified Ni foam as the outer anode, and anthracite as a fuel at 650–750 °C. The maximum power densities were 123 mW cm^{-2}, 205 mW cm^{-2}, and 378 mW cm^{-2} at 650 °C, 700 °C, and 750 °C, respectively, close to those using pure Ni foams outer anodes. This is mainly because they had the same porosity and had a good conductivity and catalytic effect in the initial stage of the test. The high performance is also in agreement with the EIS resutls under OCV conditions (Fig. 7b), of which the polarization resistances is only 0.43, 0.79, and 1.19 Ω cm^2 at 750, 700, and 650 °C, respectively.

The cell performances are very promising and also superior to previous reports of electrolyte-supported DCFCs using coal-based fuels, as shown in Table 3. The excellent performance could be mainly attributed to the 3D outer anode which expands electrochemical sites for carbon and has a positive effect on carbon gasification.
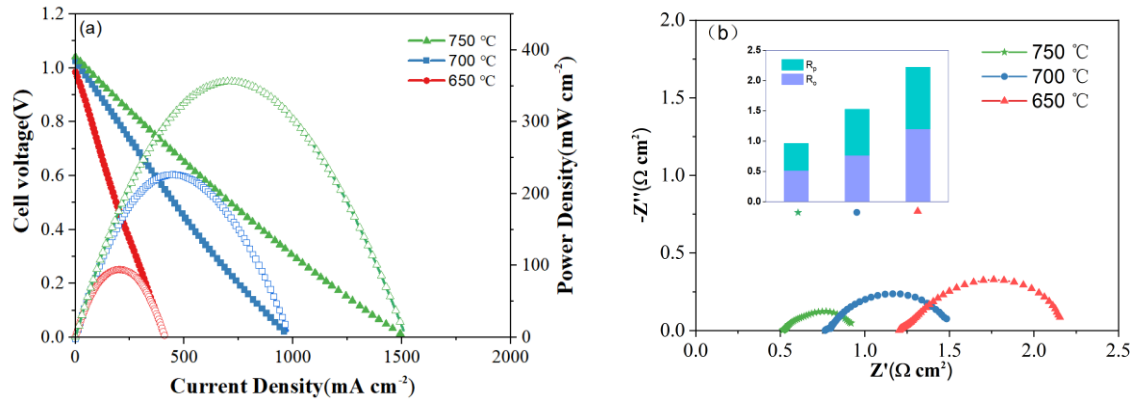

Fig. 7. Performance of HDCFCs with Cu-modified Ni foam fueled by anthracite: (a) I–V and I–P curves, (b) EIS under OCV with the corresponding ohmic resistance (R_o), and polarization resistance (RP) (inset).

Table 3

Comparison of maximum power densities of electrolyte-supported DCFCs using coal-based fuels.

Anode	Fuel	Temperature (°C)	Maximum power density (mw cm^{-2})	Ref.
$La_{0.6}Sr_{0.4}Co_{0.2}Fe_{0.8}O_3$	Morwell coal char	800	89	[42]
Ni-YSZ	Hyper-coal	811	78	[43]
Ni-YSZ/Ni-GDC	Lignite char	850	144	[44]
Ag-GDC	Brown coal char	850	221	[4]
Ni-SDC	Anthracite coal	750	306	This work
Ni-SDC-Cu@Ni foam	Anthracite coal	750	378	This work

Fig. 8 shows the discharging curve of the cells without metal foam, with Ni foam as outer anode and with Cu-modified Ni foam as outer anode using 0.6 g anthracite-carbonate as a fuel under a

galvanostatic condition of 100 mA cm^{-2} at 750 °C. The voltage plateau of the cell with Cu-modified Ni foam as the outer anode remained steady at above 0.8 V for 13 h before the drastic decrease to 0 V. In contrast, the total effective discharging time of the cells with Ni foam as the outer anode and without metal foam were only 7.5 and 2.1h, respectively. The short discharging time of the cell without metal foam is mainly due to the clogging of residual ash in the anthracite, hindering the contact of the solid carbon with the 2D anode interface. Note that in the first 4 hours the Ni foam and Cu-modified Ni foam showed a similar discharge curve, however after that the voltage of Ni foam started to decline rapidly and the Cu-modified Ni remained stable. This difference may be due to the corrosion and carbon deposition of nickel foam which in turn influences the catalytic gasification of carbon and the electron transport in 3D anode through metal skeleton. Therefore, the long discharge time of the cell with Cu-modified Ni foam as outer anode could be attributed to Cu modification and the associated improvement of coking-resistance and enhanced fuel transportation inside the 3D foam.
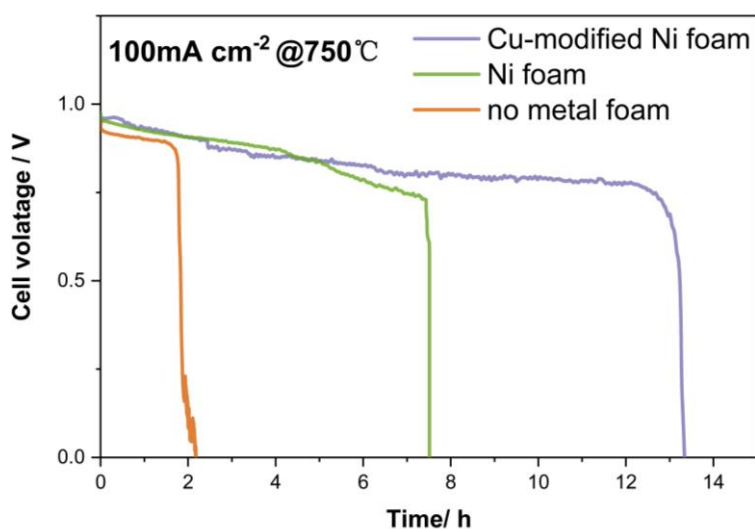

Fig. 8. Discharge curve of HDCFC fueled by 0.6 g coal-carbonate mixture.

Fig. 9a and Fig. 9b show the morphologies of the metal foam before and after the test, respectively. The mixture of anthracite and carbonate initially filled the entire metal foam before the test because the particle size of the mixture was much smaller than the pore size of the metal foam. After the discharge, most of the fuel had been consumed, leaving only some ash on the metal foam skeleton instead of thorough coverage in traditional HDCFC that is expected to passivate the anode and coal from deep discharge. In addition, the metal foam maintained its

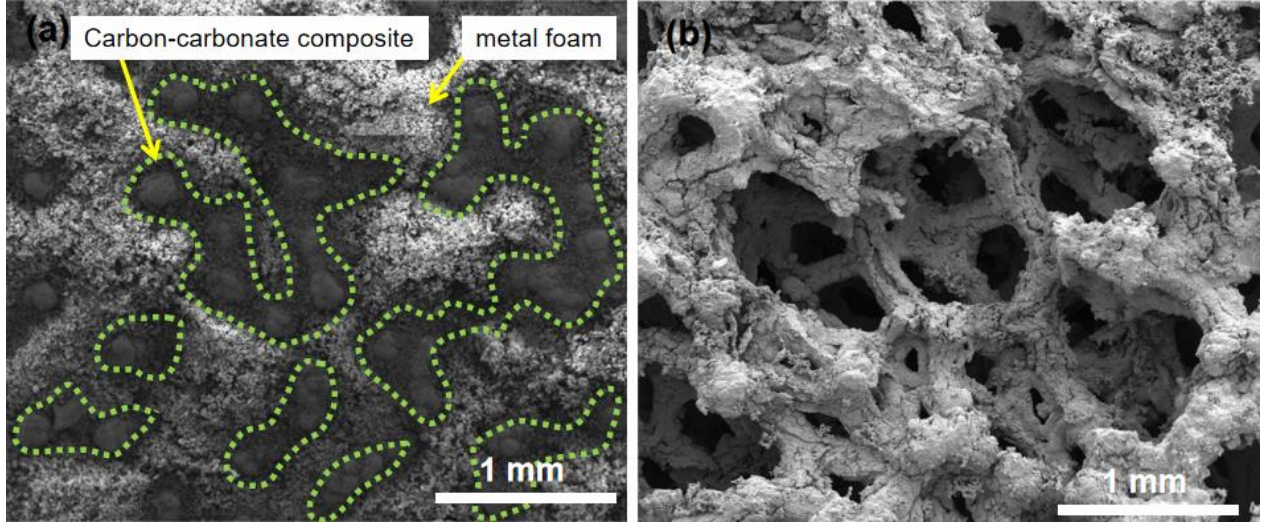original 3D morphology, reflecting its good mechanical properties and stability.

Fig. 9. SEM images of the Cu-modified Ni foam before (a) and after (b) discharge test.

To further evaluate the applicability of the cell with Cu-modified Ni foam as an outer anode, the fuel utilization (η) was calculated for the discharge test according to the following equation:

$$\eta = \frac{n_{C^{electricity}}}{n_{C^{total}}} \times 100\% = \frac{\dfrac{It}{zF}}{\dfrac{m}{M}} \times 100\% = \frac{ItM}{zFm} \times 100\% \tag{5}$$

where *I*, *t*, *M*, *m*, *F*, and *z* represent the operation current, discharge time, molecular weight of carbon, mass of feeding carbon fuel, Faraday's constant (96,485 C mol^{-1}), and electron transfer number, respectively. In the electrochemical oxidation of carbon fuel, z = 2 and z = 4 occur simultaneously, corresponding to the incomplete electrochemical oxidation of carbon (Eq. 2, Eq. 4, Eq. 6) and complete electrochemical oxidation of carbon (Eq. 1 and Eq. 3), respectively. The calculated fuel utilization was between 21.5% and 43% according to Eq. (5). Considering that this HDCF was fueled with raw coal and CO, the CO_2 generated from coal gasification left the fuel cell compartment during the heating and testing process; such a fuel utilization is highly attractive. It can be perceived that at the early stage of the discharge test, the main anodic reaction is the electrochemical oxidation of C to CO_2. With the continuous consumption of carbon, the accumulation of ash hinders the contact between the carbon and the electrolyte, and thus the electrochemical oxidation of C to CO became the primary path due to insufficient supply of

oxygen ions. Inevitable CO run away, therefore, becomes substantial and degrades the efficiency. Based on this, there is much potential to further increase fuel utilization and energy efficiency by preventing the deposition of ash on the anode, e.g. by manufacturing cathode-supported tubular HDCFCs, or employing energy harvest from the CO in the flue gas.

Conclusions

In summary, we developed a Cu-modified Ni foam 3D anode for high-performance HDCFCs. The metal foam extended the anode space from the interface between the Ni/SDC and the fuel anode to the entire 3D anode where the metal foam was located, promoting the electrochemical oxidation of carbon. During the discharge test, the ash was evenly distributed on the metal foam skeleton instead of accumulated on the surface of the traditional anode, which effectively improves the stability of the cell. The CuNi alloy layer formed on the surface of the Ni foams exhibited excellent coke-resistance in the anthracite-carbonate mixture under high temperature. The anthracite-fueled HDCFC using Cu-modified Ni foam as a 3D anode showed a maximum power density of 378 mW cm^{-2} at 750 °C. Considering that the cell is electrolyte-supported, this performance is highly encouraging. In addition, the cell reached stable operation for more than 13 h at 100 mA cm^{-2} when using 0.6g coal-carbonate mixture as fuel. This work highlights that the development of 3D anodes would have great feasibility in the application of HDCFCs.

References

[1] H. Xie, S. Zhai, B. Chen, T. Liu, Y. Zhang, M. Ni, Z. Shao, Coal pretreatment and Ag-infiltrated anode for high-performance hybrid direct coal fuel cell, Appl. Energy (2020) 114197, https://doi.org/10.1016/j.apenergy.2019.114197.

[2] G. Zhang, T. Guan, N. Wang, J. C. Wu, J. L. Wang, J. L. Qiao, K. X. Li, Small mesopore

engineering of pitch-based porous carbons toward enhanced supercapacitor performance, Chem. Eng. J. (2020) 125818, https://doi.org/10.1016/j.cej.2020.127010.

[3] Y. Jiao, J. Zhao, W. An, L. Zhang, Y. Sha, G. Yang, Z. Shao, Z. Zhu, S. D. Li, Structurally modified coal char as a fuel for solid oxide-based carbon fuel cells with improved performance, J. Power Sources 288 (2015) 106–114, https://doi.org/10.1016/j.jpowsour.2015.04.121.

[4] H. Wu, J. Xiao, X. Zeng, X. Li, J. Yang, Y. Zou, S. Liu, P. Dong, Y. Zhang, J. Liu, A high performance direct carbon solid oxide fuel cell–A green pathway for brown coal utilization, Appl. Energy 248 (2019) 679–87, https://doi.org/10.1016/j.apenergy.2019.04.104.

[5] H. Jang, Y. Park, J. Lee, Origin of peculiar electrochemical phenomena in direct carbon fuel cells, Chem. Eng. J. 327 (2017) 1163−1175, https://doi.org/10.1016/j.cej.2017.06.127.

[6] C. Liu, J. Pu, X. Chen, Z. Ma, X. Ding, J. Zhou, S. Wang, High-performance gas–electricity cogeneration using a direct carbon solid oxide fuel cell fueled by biochar derived from camellia oleifera shells, Int. J. Hydrogen Energy (2020) 11784, https://doi.org/10.1016/j.ijhydene.2020.07.214.

[7] A. C. Rady, S. Giddey, A. Kulkarni, S. P. Badwal, S. Bhattacharya, Catalytic gasification of carbon in a direct carbon fuel cell, Fuel 180 (2016) 270–7, https://doi.org/10.1016/j.fuel.2016.04.047.

[8] J. Wang, H. Chen, Y. Tian, M. Yao, Y. Li, Thermodynamic analysis of hydrogen production for fuel cells from oxidative steam reforming of methanol, Fuel 97 (2012) 805, https://doi.org/10.1016/j.fuel.2012.03.008.

[9] W. Cai, Q. Zhou, Y. Xie, J. Liu, A facile method of preparing Fe-loaded activated carbon fuel for direct carbon solid oxide fuel cells, Fuel 159 (2015) 887–893, https://doi.org/10.1016/j.fuel.2015.07.030.

[10] J. Allen, M. Glenn, S. Donne, Analysis of theoretical efficiency in a model 10 kW direct carbon fuel cell using a coal based carbonate slurry, Electrochim. Acta (2020) 135131, https://doi.org/10.1016/j.electacta.2019.135131.

[11] A. Fuente-Cuesta, C. Jiang, A. Arenillas, J. T. Irvine, Role of coal characteristics in the electrochemical behaviour of hybrid direct carbon fuel cells, Energy Environ. Sci. 9 (2016) 2868–2680, https://doi.org/10.1039/c6ee01461e.

[12] K. Bie, P. Fu, Y. Liu, Muhammad, Comparative study on the performance of different carbon fuels in a molten carbonate direct carbon fuel cell with a novel anode structure, J. Power Sources 460 (2020) 228101, https://doi.org/10.1016/j.jpowsour.2020.228101.

[13] X. Xu, W. Zhou, F. Liang, Z. Zhu, A comparative study of different carbon fuels in an electrolyte-supported hybrid direct carbon fuel cell, Appl. Energy 108 (2013) 402–409, https://doi.org/10.1016/j.apenergy.2013.03.053.

[14] W. Zhou, Y. Jiao, S. D. Li, Z.Shao, Anodes for Carbon–Fueled Solid Oxide Fuel Cells,

ChemElectroChem, 3.2 (2016) 193–203, https://doi.org/10.1002/celc.201500420.

[15] M. Ma, X. Yang, J. Qiao, W. Sun, Z. Wang, K. Sun, Progress and challenges of carbon-fueled solid oxide fuel cells anode, Journal of Energy Chemistry (2020), https://doi.org/10.1016/j.jechem.2020.08.013.

[16] J. Liu, H. Yuan, J. Qiao, J. Feng, C. Xu, Z. Wang, K. Sun Hierarchical hollow nanofiber networks for high-performance hybrid direct carbon fuel cells, J. Mater. Chem. A 5 (2017) 17216–17220, https://doi.org/10.1039/c7ta04616b.

[17] W. Wu, Y. Zhang, D. Ding, T. He, A high–performing direct carbon fuel cell with a 3D architectured anode operated below 600 °C, Advanced Materials 30.4 (2018) 1704745, https://doi.org/10.1002/adma.201704745.

[18] M. Ma, X. Yang, R. Ren, C. Xu, J. Qiao, W. Sun, K. Sun, Z. Wang, Honeycombed Porous, Size-Matching Architecture for High-Performance Hybrid Direct Carbon Fuel Cell Anode, ACS Appl. Mater. Interfaces 12.27 (2020) 30411–30419, https://doi.org/10.1021/acsami.0c02866.

[19] W. C. Tan, L. H. Saw, H. San Thiam, J. Xuan, Z. Cai, M. C. Yew. Overview of porous media/metal foam application in fuel cells and solar power systems, Renew Sustain Energy Rev (2018) 96:181–197, https://doi.org/10.1016/j.rser.2018.07.032.

[20] N. Yan, X. Z. Fu, J. L. Luo, K. T. Chuang, A. R. Sanger. Ni–P coated Ni foam as coking resistant current collector for solid oxide fuel cells fed by syngas, J. Power Sources 198 (2012) 164–169, https://doi.org/10.1016/j.jpowsour.2012.01.110.

[21] J. Yu, F. Chen, Q. Tang, T. T. Gebremariam, J. Wang, X. Gong, X. Wang. Ag-modified Cu foams as three-dimensional anodes for rechargeable zinc-air batteries, ACD Appl. Nano Mater. 2 (2019) 2679–2688, https://doi.org/10.1021/acsanm.9b00156.

[22] G. Yang, J. Chen, P. Xiao, P. O. Agboola, I. Shakir, Y. Xu, Graphene anchored on Cu foam as a lithiophilic 3D current collector for a stable and dendrite-free lithium metal anode, J. Mater. Chem. A 6 (2018) 9899–9905, https://doi.org/10.1021/acsanm.9b00156.

[23] G. J. Davies, S. Zhen, Metallic foams: their production, properties and applications, J. Mater. Sci. 18 (1983) 1899–1911, https://doi.org/10.1007/bf00554981.

[24] B. Hua, M. Li, Y. Q. Zhang, J. Chen, Y. F. Sun, N.Yan, J. Li, J. L. Luo, Facile synthesis of highly active and robust Ni-Mo bimetallic electrocatalyst for hydrocarbon oxidation in solid oxide fuel cells, ACS Energy Letters 1.1 (2016) 225–230.

[25] H. Gu, R. Ran, W. Zhou, Z. Shao, Anode-supported ScSZ-electrolyte SOFC with whole cell materials from combined EDTA–citrate complexing synthesis process, J. Power Sources 172 (2007) 704–712, https://doi.org/10.1016/j.jpowsour.2007.07.056.

[26] W. Bian, W. Wu, C. J. Orme, H. Ding, M. Zhou, D. Ding, Dual 3D Ceramic Textile Electrodes: Fast Kinetics for Carbon Oxidation Reaction and Oxygen Reduction Reaction in Direct Carbon Fuel Cells at Reduced Temperatures, Advanced Functional Materials 30.19 (2020) 1910096, https://doi.org/10.1002/adfm.201910096.

[27] A. C. Rady, S. Giddey, S. P. Badwal, B. P. Ladewig, S. Bhattacharya, Review of fuels for direct carbon fuel cells, 26.3 Energy & Fuels (2012) 1471–1488.

[28] L. Deleebeeck, K. Kammer Hansen, Hybrid direct carbon fuel cells and their reaction mechanisms—a review, 18.4 Journal of Solid State Electrochemistry (2014) 861–882.

[29] L. Deleebeeck, D. Ippolito, K. Kammer Hansen, Enhancing hybrid direct carbon fuel cell anode performance using Ag_2O, 152 Electrochimica Acta (2015) 222–239, https://doi.org/10.1016/j.electacta.2014.11.064861–882.

[30] C. Jiang, J. Ma, A. D. Bonaccorso, J. T. Irvine, Demonstration of high power, direct conversion of waste-derived carbon in a hybrid direct carbon fuel cell, Energy Environ. Sci. 5.5 (2012) 6973–6980, https://doi.org/10.1039/c2ee03510c.

[31] X. Li, Z. Zhu, J. Chen, R. De Marco, A. Dicks, J. Bradley, G. Lu, Surface modification of carbon fuels for direct carbon fuel cells, J. Power Sources 186 (2009) 1–9, https://doi.org/10.1016/j.jpowsour.2008.09.070.

[32] X. Xu, W. Zhou, F. Liang, Z. Zhu, Optimization of a direct carbon fuel cell for operation below 700°C, Int. J. Hydrog. Energy 38 (2013) 5367–5374, https://doi.org/10.1016/j.ijhydene.2013.02.066.

[33] X. Yue, A. Arenillas, J. T. Irvine, Application of infiltrated LSCM-GDC oxide anode in direct carbon/coal fuel cells, Faraday Discuss 190 (2016) 269–289, https://doi.org/10.1039/c6fd00001k.

[34] H. Xu, B. Chen, H. Zhang, P. Tan, G. Yang, J. T. Irvine, M. Ni, Experimental and modeling study of high performance direct carbon solid oxide fuel cell with in situ catalytic steam-carbon gasification reaction, J. Power Sources, (2018) 135–143, https://doi.org/10.1016/j.jpowsour.2018.02.033.

[35] K. Sun, J.Liu, J.Feng, H.Yuan, M. He, C. Xu, Z. Wang, W. Sun, J. Qiao, Investigation of B-site doped perovskites $Sr_2Fe_{1.4}X_{0.1}Mo_{0.5}O_{6-\delta}$ (X=Bi, Al, Mg) as high-performance anodes for hybrid direct carbon fuel cell, J. Power Sources 365 (2017) 109–116, https://doi.org/10.1016/j.jpowsour.2017.08.083.

[36] J. Lu, C. Zhu, C. Pan, W. Lin, J. P. Lemmon, F. Chen, C. Li, K. Xie, Highly efficient electrochemical reforming of CH_4/CO_2 in a solid oxide electrolyser, Sci. Adv. 4 (2018) eaar5100, https://doi.org/10.1126/sciadv.aar5100.

[37] Z. Xie, C. Xia, M. Zhang, W. Zhu, H. Wang, $Ni_{1-x}Cu_x$ alloy-based anodes for low-temperature solid oxide fuel cells with biomass-produced gas as fuel, J. Power Sources 161 (2006) 1056–1061, https://doi.org/10.1016/j.jpowsour.2006.05.025.

[38] Q. X. Low, W. Huang, X. Z. Fu, J. Melnik, J. L. Luo, K. T. Chuang, A. R. Sanger, Copper coated nickel foam as current collector for H_2S-containing syngas solid oxide fuel cells, Appl. Surface Sci. 258 (2011) 1014–1020, https://doi.org/10.1016/j.apsusc.2011.07.133.

[39] J. Wu, G. Gao, J. Li, P. Sun, X. Long, F. Li, Efficient and versatile CuNi alloy nanocatalysts

for the highly selective hydrogenation of furfural, Appl. Catalysis B-environmental 203 (2017) 227–236, https://doi.org/10.1016/j.apcatb.2016.10.038

[40] W. Cai, J. Liu, P. Liu, Z. Liu, H. Xu, B. Chen, Y. Li, Q. Zhou, M. Liu, M. Ni, A direct carbon solid oxide fuel cell fueled with char from wheat straw, International Journal of Energy Research, 43.7 (2019) 2468–2477, https://doi.org/10.1002/er.3968.

[41] M. Ma, J. Qiao, X. Yang, C. Xu, R. Ren, W. Sun, K. Sun, Z. Wang, Enhanced Stability and Catalytic Activity on Layered Perovskite Anode for High-Performance Hybrid Direct Carbon Fuel Cells, ACS Appl. Materials & Interfaces 12.11 (2020).12938–12948, https://dx.doi.org/10.1021/acsami.0c02866.

[42] A. C. Rady, S. Giddey, A. Kulkarni, S. P. S. Badwal, S. Bhattacharya, B. P. Ladewig, Direct carbon fuel cell operation on brown coal, Appl. Energy 120 (2014) 56–64, https://doi.org/10.1016/j.apenergy.2014.01.046.

[43] M. Dudek, P. Tomczyk, R. Socha, M. Hamaguchi, Use of ash-free″Hyper-coal″as a fuel for a direct carbon fuel cell with solid oxide electrolyte, Int. J. Hydrogen Energy 39.23 (2014) 12386–12394, https://doi.org/10.1016/j.ijhydene.2014.04.057

[44] J. Jewulski, M. Skrzypkiewicz, M. Struzik, I. Lubarska-Radziejewska, Lignite as a fuel for direct carbon fuel cell system, Int. J. Hydrogen Energy 39 (2014) 21778–85, https://doi.org/10.1016/j.ijhydene.2014.05.039.